

1 **A method for merging nadir-sounding climate records,**
2 **with an application to the global-mean stratospheric**
3 **temperature data sets from SSU and AMSU**

4 (revised June 28, 2015)
5

6 **C. McLandress¹, T. G. Shepherd², A. I. Jonsson¹, T. von Clarmann³ and B.**
7 **Funke⁴**

8 [1]{Department of Physics, University of Toronto, Toronto, Canada}

9 [2]{Department of Meteorology, University of Reading, Reading, UK}

10 [3]{Karlsruhe Institute of Technology, Karlsruhe, Germany}

11 [4]{Instituto de Astrofísica de Andalucía, Granada, Spain}

12
13 **Abstract**

14 A method is proposed for merging different nadir-sounding climate data records
15 using measurements from high resolution limb sounders to provide a transfer
16 function between the different nadir measurements. The two nadir-sounding
17 records need not be overlapping so long as the limb-sounding record bridges
18 between them. The method is applied to global mean stratospheric temperatures
19 from the NOAA Climate Data Records based on the Stratospheric Sounding Unit (SSU)
20 and the Advanced Microwave Sounding Unit-A (AMSU), extending the SSU record
21 forward in time to yield a continuous data set from 1979 to present, and providing a
22 simple framework for extending the SSU record into the future using AMSU. SSU and
23 AMSU are bridged using temperature measurements from the Michelson
24 Interferometer for Passive Atmospheric Sounding (MIPAS), which is of high enough
25 vertical resolution to accurately represent the weighting functions of both SSU and
26 AMSU. For this application, a purely statistical approach is not viable since the
27 different nadir channels are not sufficiently linearly independent, statistically
28 speaking. The near-global mean linear temperature trends for extended SSU for
29 1980-2012 are -0.63 ± 0.13 , -0.71 ± 0.15 and -0.80 ± 0.17 K decade⁻¹ (95%

30 confidence) for channels 1, 2 and 3, respectively. The extended SSU temperature
31 changes are in good agreement with those from the Microwave Limb Sounder (MLS)
32 on the Aura satellite, with both exhibiting a cooling trend of $\sim 0.6 \pm 0.3$ K decade⁻¹ in
33 the upper stratosphere from 2004-12. The extended SSU record is found to be in
34 agreement with high-top coupled atmosphere-ocean models over the 1980-2012
35 period, including the continued cooling over the first decade of the 21st century.

36

37 **1 Introduction**

38 Stratospheric cooling has long been regarded as a key indicator of two anthropo-
39 genic climate forcings (IPCC 2013; WMO 2014): that from increasing abundances of
40 CO₂, and that from the ozone decline associated with the increased abundances of
41 ozone-depleting substances (ODSs). The former has continued secularly, while the
42 latter peaked in the late 1990s and has been slowly declining since then. Thus, the
43 contrast between the early and more recent parts of the stratospheric temperature
44 record is an important fingerprint of anthropogenic influence (Shepherd and
45 Jonsson, 2008). In addition to the anthropogenic influences, stratospheric tempera-
46 ture is also strongly perturbed by the 11-year solar cycle and by volcanic eruptions.
47 As a consequence, the anthropogenic cooling is considerably modulated in time.

48 In the stratosphere, global mean temperature is, to a first approximation, unaffected
49 by dynamics and is therefore close to radiative equilibrium (Fomichev, 2009). This
50 makes it an ideal quantity for detection and attribution of anthropogenic influence
51 (Shine et al., 2003). However, global averages are only obtainable from satellites,
52 and the only long-term satellite record of stratospheric temperature is that from the
53 operational nadir sounders, the Stratospheric Sounding Unit (SSU)/Microwave
54 Sounding Unit (MSU) and the Advanced Microwave Sounding Unit-A (henceforth
55 AMSU) (Randel et al., 2009), which represent deep atmospheric layers. Note that the
56 vertically resolved temperature data from Global Positioning System (GPS) radio
57 occultation only begin in the current century (Wickert et al., 2001), and do not reach
58 into the upper stratosphere, where the strongest cooling is found. The nadir soun-

59 ding measurements were never designed for climate monitoring, and homogenizing
60 the data from different operational satellites, with rapidly drifting orbits, is a
61 challenge (Wang et al., 2012; Zou et al., 2014; Nash and Saunders, 2015).

62 In the lower stratosphere, the relevant nadir record is provided by MSU channel 4
63 (and continued by AMSU channel 9; Christy et al., 2003; Mears et al., 2009) and is
64 supplemented by radiosondes and, since the early 2000s, by GPS radio occultation.
65 The global-mean MSU4 record is considered fairly reliable and most attention has
66 focused on its latitudinal structure (Randel et al., 2009).

67 The middle and upper stratosphere is, however, a completely different story. There
68 the nadir record is provided by three SSU channels which began in 1979 and ended
69 in 2006, and by six AMSU channels which began in 2001 and are ongoing. Because
70 the weighting functions of the SSU and AMSU channels are very different, the two
71 records cannot be immediately combined. Moreover, confidence in the SSU record
72 has been low, even for global-mean temperature, because of the lack of corrobor-
73 ative measurements, drift issues within the SSU record itself, and the striking dif-
74 ferences identified by Thompson et al. (2012) between the two SSU products avail-
75 able at that time [from the National Oceanic and Atmospheric Administration
76 (NOAA) and the Met Office] and between the measurements and chemistry-climate
77 models.

78 Normally, differences between measurements and models would tend to cast sus-
79 picion on the models, not the measurements. However, because global-mean strato-
80 spheric temperature is radiatively controlled, its behaviour in the middle and upper
81 stratosphere, where the radiative processes are well understood, should be
82 reasonably well represented by chemistry-climate models. Indeed, Fig. 2 of
83 Thompson et al. (2012) shows that for the SSU channels the differences in cooling
84 between models and observations, and between the Met Office and NOAA products
85 of the time, are in almost all cases much larger than the inter-model spread. One of
86 the mysteries arising from Thompson et al. (2012) was the apparent lack of
87 continued cooling in the SSU record during the early 2000s, in contrast to the

88 models and in contradiction to physical expectations. Because the SSU record ended
89 in 2005, this mystery was unresolved.

90 The large differences between the NOAA SSU results and models found by Thomp-
91 son et al. motivated the development of a revised version of NOAA SSU (version 2),
92 the results of which are published in Zou et al. (2014). The version 2 global-mean
93 temperatures exhibit weaker long-term cooling trends than the version 1
94 temperatures that are shown in Thompson et al. (by ~30% for channels 1 and 3 and
95 ~17% for channel 2). Although Zou et al. did not compare their results to models,
96 visual inspection of their version 2 temperatures indicates much closer agreement
97 with the model results shown in Thompson et al. (2012). There has also been a
98 subsequent revision of the Met Office data set (Nash and Saunders, 2015).

99 In this paper, we propose a method for merging different nadir-sounding climate
100 data records, and apply it to the NOAA SSU and AMSU global-mean stratospheric
101 temperature records. Specifically we use the AMSU data to extend the three SSU
102 channels forward in time, given the paradigmatic importance of that climate data
103 record. We show that a purely statistical approach, using multiple linear regression,
104 is unworkable for this particular application since the six AMSU channels are not
105 sufficiently linearly independent. Instead, we propose a physically based method
106 using limb-sounding measurements, with much higher vertical resolution, to
107 accurately represent the weighting functions of both SSU and AMSU, and thereby act
108 as a transfer function between the two nadir-sounding data sets. For this purpose
109 we use temperature data from the Michelson Interferometer for Passive
110 Atmospheric Sounding (MIPAS). It is important to emphasize that the merged data
111 set can only be as good as the component data sets going in, and relies on the
112 extensive efforts spent on homogenizing the SSU and AMSU data records
113 themselves.

114 Since we are dealing with monthly-mean, global-mean data, the data are highly
115 averaged and the effect of random measurement errors is expected to be low.
116 Characterization of the systematic errors in such highly averaged quantities in a

117 bottom-up fashion would be extremely challenging (Hegglin et al., 2013). Instead,
118 our approach is to compare the different data sets (after transformation via the
119 weighting functions) over their overlap periods to see whether the differences
120 between them can be characterized in terms of a constant offset (within some
121 noise). If this is the case, then the merging can be done with confidence. Thus, the
122 validity of the approach can be assessed a posteriori. This approach was followed by
123 Hegglin et al. (2014) in constructing a merged stratospheric water vapour record.
124 Solomon et al. (2010) also performed such an additive relative bias correction to
125 merge the HALOE and MLS stratospheric water vapour records. Thus there is ample
126 precedent for such an approach in the literature.

127 The data sets used are described in Sect. 2. The merging methodology and the
128 comparison between MIPAS and the two nadir sounding records are provided in
129 Sect. 3.1. This comparison shows that the different global-mean data sets track each
130 other very well, so additive relative biases can be identified with small uncertainties.
131 Section 3.2 examines the (near) global-mean temperature trends, both over the
132 recent record (as represented by the six AMSU channels) where we compare the
133 MIPAS and AMSU trends to those from the Microwave Limb Sounder (MLS) on the
134 Aura satellite, and over the extended SSU record. The extended SSU record is found
135 to be in agreement with high-top coupled atmosphere-ocean models over the 1980-
136 2012 period, including the continued cooling over the first decade of the 21st
137 century. Conclusions are drawn in Sect. 4.

138

139 **2 Description of data sets**

140 **2.1 SSU**

141 SSU is a three-channel infrared radiometer on board a series of NOAA satellites
142 which measures temperatures over deep layers in the stratosphere. The near-global
143 ($\sim 85^{\circ}\text{S}$ to 85°N) data set extends from 1979 until early 2006. We use Version 2
144 brightness temperatures (Zou et al., 2014), as well as the weighting functions for the

145 three channels. The data set is produced by the NOAA Center for Satellite
146 Applications and Research (STAR) and is available at
147 ftp://ftp.star.nesdis.noaa.gov/pub/smcd/emb/mscat/data/SSU/SSU_v2.0/.

148 As stated in the Introduction, Version 2 was developed primarily as a result of the
149 large differences found between SSU Version 1 (Wang et al., 2012) and a Met Office
150 version of SSU, as well as between SSU Version 1 and models, that were documented
151 in Thompson et al. (2012). Differences from Version 1 include improvements in the
152 radiance calibration and in the adjustments for diurnal drift and intersatellite
153 biases. Please refer to Zou et al. (2014) for an in-depth discussion of the differences.

154

155 **2.2 AMSU**

156 AMSU-A is a microwave radiometer on board a series of recent, current and future
157 NOAA satellites. It has 11 channels, 6 of which (channels 9 to 13) provide coverage
158 in the stratosphere. The instrument was first launched in 1998, although not all of
159 the stratospheric channels were in operation until 2001. We use brightness
160 temperatures analyzed by NOAA STAR (Wang and Zou, 2014), which are available at
161 ftp://ftp.star.nesdis.noaa.gov/pub/smcd/emb/mscat/data/AMSU_v1.0/monthly.

162 The corresponding weighting functions for channels 9 to 14 were provided courtesy
163 of Likun Wang of NOAA STAR. The temperature data for channels 9 to 13 start in
164 January 1999; those for channel 14 start two years later. As with SSU, the AMSU data
165 extend from $\sim 85^{\circ}\text{S}$ to 85°N .

166

167 **2.3 MIPAS**

168 MIPAS is a limb sounder which measured infrared emission from which vertical
169 profiles of temperature and atmospheric constituents are derived (Fischer et al.,
170 2008). We use zonal and monthly mean gridded temperatures computed from
171 versions V3o_T_10 and V5r_T220 for the periods 2002-2004 and 2005-2011,
172 respectively. These data are available at [http://www.esa-spin.org/index.php/spin-](http://www.esa-spin.org/index.php/spin-data-sets)
173 [data-sets](http://www.esa-spin.org/index.php/spin-data-sets) and are provided on a 5-degree latitude grid from $\sim 75^{\circ}\text{S}$ to 75°N with 28
174 pressure levels ranging from 300 hPa to 0.1 hPa. The parent data were produced by

175 the Institute for Meteorology and Climate Research at Karlsruhe Institute of
176 Technology, in cooperation with the Institute of Astrophysics of Andalusia, from
177 calibrated radiance spectra provided by the European Space Agency. The MIPAS
178 temperature retrieval method is discussed in von Clarmann et al. (2003) for the high
179 spectral resolution measurement period until 2004 and in von Clarmann et al.
180 (2009) for the reduced spectral resolution measurement period from 2005
181 onwards. MIPAS temperatures have been validated by Wang et al. (2005) and Stiller
182 et al. (2012).

183

184 **2.4 MLS**

185 Aura MLS is a limb sounder that measures thermal microwave emission. It has
186 provided a nearly continuous set of measurements of temperature and trace gases
187 in the middle atmosphere since August 2004. The data extend near globally and
188 from the middle troposphere to the lower thermosphere. We use version 3.3
189 temperature data (Livesey et al., 2011) through the end of 2011. The temperature
190 retrieval method and validation are discussed in Schwartz et al. (2008).

191

192 **2.5 CMAM30**

193 The CMAM30 data set, which extends from 1979 to 2011, is produced using a
194 specified-dynamics version of the Canadian Middle Atmosphere Model (CMAM) that
195 is driven by winds and temperatures from the interim version of the European
196 Centre for Medium-Range Weather Forecasts Reanalysis (ERA Interim; Dee et al.,
197 2011), where the global mean temperatures have been adjusted in the upper
198 stratosphere to remove temporal discontinuities in 1985 and 1998 that have arisen
199 from the introduction of new satellite data in the assimilation process (McLandress
200 et al., 2014). Here we use the monthly mean CMAM30 temperatures, which are
201 available at

202 <http://www.cccma.ec.gc.ca/data/cmam/output/CMAM/CMAM30-SD/mon/atmos/>.

203

204

205 **2.6 CMIP5**

206 Coupled atmosphere-ocean models from phase 5 of the Coupled Model Intercom-
207 parison Project (CMIP5) are also examined. Most of these models are not chemistry-
208 climate models and do not have upper boundaries extending high into the
209 stratosphere or above. The nine models that are used are listed in Table 1. To span
210 the period extending from 1979 to 2012 data from the historical experiment
211 (ending December 2005) and the Representative Concentration Pathway (RCP) 4.5
212 experiment (a projection starting in January 2006) are employed. Since the RCP 4.5
213 simulations use as initial conditions data from the end of the historical simulations,
214 the two simulations for a given model are continuous and, thus, can be simply
215 concatenated to produce a single time series. Since we use only the first few years of
216 the RCP 4.5 simulation, differences between it and the three other RCP simulations
217 (RCP 2.5, 6 and 8.5) are expected to be very small. Following Thompson et al. (2012)
218 the SSU channels onto which the data are projected depend on the height of the top
219 model data level: channel 1 (any model with data at 1 hPa), channels 1 and 2 (any
220 model with data at pressure levels below 1 hPa), and channels 1-3 (any model with
221 data at pressure levels below 0.1 hPa).

222

223 **2.7 CCMVal2**

224 Chemistry-climate model (CCM) simulations of the recent past from phase 2 of the
225 CCM Validation project (CCMVal2) are used. These REF-B1 simulations use observed
226 sea-surface temperatures and sea-ice distributions and observed forcings (volcanic
227 aerosols, tropospheric concentrations of greenhouse gases, ozone-depleting sub-
228 stances, and solar variations). The data are available at the SPARC Data Center at
229 <http://www.sparc-climate.org/data-center/data-access/>. The following 16 models,
230 all with model tops above 1 hPa, were used: AMTRAC3, CCSRNIES, CMAM, CNRM-
231 ACM, EMAC, EMAC-FUB, GEOSCCM (and hist-GEOSCCM), LMDZrepro, MRI, Niwa-
232 SOCOL, SOCOL, ULAQ, UMETRAC, UМУKCA-METO, UМУKCA-UCAM and WACCM,
233 where the model acronyms are defined in Morgenstern et al. (2010). Two models
234 (CAM3.5 and E39C) were excluded because their upper boundaries were at heights

235 above 1 hPa. A third model (UMSLIMCAT) was excluded because the file containing
236 the zonal and monthly mean temperature data did not have a latitude array. For
237 model data sets containing a missing data flag for points below ground, those points
238 were filled using temperatures from the first good data point above. Since such
239 points occur at high latitudes (Antarctica) and at pressure levels corresponding to
240 altitudes far below the peak of the SSU weighting functions, their impact on the SSU-
241 weighted near global mean is negligible. The CCMVal2 models are described in
242 Morgenstern et al. (2010).

243

244 **3 Results**

245 The results section is divided into two parts. The first part (Sect. 3.1) pertains to the
246 merging of the SSU and AMSU data sets. Since this is achieved using MIPAS data as a
247 transfer function, we begin by demonstrating that MIPAS is in good agreement with
248 SSU and AMSU. We then describe the algorithm used to merge SSU and AMSU, and
249 present the merged results. The second part (Sect. 3.2) is an analysis of temperature
250 trends for the post-2000 time period when the AMSU, MIPAS and MLS data are all
251 available, as well as a comparison of our “extended” SSU results to other long term
252 data sets, including models. All results presented here are for monthly and near-
253 global means (75°S-75°N). This particular latitude range is dictated by the use of the
254 MIPAS data in merging the SSU and AMSU data sets.

255

256 **3.1 Merging SSU and AMSU**

257 **3.1.1 Comparisons to MIPAS**

258 In order to compare MIPAS to SSU and AMSU, the MIPAS temperatures must be
259 averaged in the vertical using the SSU and AMSU weighting functions, which are
260 shown in the left and right panels of Fig. 1, respectively (thick solid curves). For
261 simplicity we follow Thompson et al. (2012) in using fixed weighting functions,
262 rather than attempting to account for possible state-dependence. The three SSU
263 weighting functions (channels 1-3) peak at approximately ~30, 39 and 44 km. The
264 six stratospheric AMSU weighting functions (channels 9-14) peak at ~17, 20, 25, 30,

265 37 and 42 km. The other curves in the left panel of Fig. 1 will be discussed in due
266 course.

267 The vertical averaging is performed on a log-pressure height grid, with the limits of
268 integration being the corresponding height range of the MIPAS data: 300 hPa (~ 8.4
269 km) and 0.1 hPa (~ 64.5 km). The vertically averaged temperature for channel n
270 (denoted T_n) is therefore given by

$$271 \quad T_n(t) = \int_{z_b}^{z_t} T(t, z) W_n(z) dz \quad (1)$$

272 where t is time in month and z is the log-pressure height [$z = -H \ln(p/p_s)$, with $H =$
273 7 km and $p_s = 1000$ hPa], and z_b and z_t are the limits of integration, namely $z(300$
274 hPa) and $z(0.1$ hPa). Before computing the vertical average, the weighting functions
275 are normalized so that their vertical integral from z_b to z_t equals 1.

276 By excluding the lower troposphere and upper mesosphere in Eq. (1), the full
277 vertical integrals of the weighting functions are approximated. This approximation
278 is less accurate for SSU than it is for AMSU since the SSU weighting functions extend
279 down lower and up higher than for AMSU (Fig. 1). To investigate the possible impact
280 of this incomplete vertical averaging using the SSU weighting functions, we first
281 filled the MIPAS temperature data below 300 hPa and above 0.1 hPa using the
282 corresponding CMAM30 data, and then performed the integration using $z_b = 0$ km to
283 $z_t \cong 100$ km. The resulting vertically averaged temperatures for the three SSU chan-
284 nels (not shown) are virtually indistinguishable from those obtained by averaging
285 only over the MIPAS domain (8-65 km), leading us to conclude that the effect of the
286 incomplete vertical sampling of the integral given by Eq. (1) is negligible.

287 Figure 2 compares the SSU-weighted MIPAS temperatures to SSU for 2002-2007, the
288 years when the two instruments overlap. The thick and thin lines denote,
289 respectively, the results with and without the seasonal cycle included, where the
290 seasonal cycle is given by the first three harmonics of the annual cycle. The MIPAS
291 time series have each been offset by a constant amount with respect to SSU, with the
292 offset being determined so that the mean difference between the deseasonalized

293 MIPAS and SSU time series is zero over the 4-year overlap period. The offsets are
 294 small: ~ -0.2 K for channels 1 and 3 and ~ -0.7 K for channel 2. There is very good
 295 agreement between MIPAS and SSU for the seasonal cycle; however, as will be
 296 discussed later, the MIPAS data exhibit a larger trend than does SSU (see Fig. 9).

297 Figure 3 shows the corresponding results for AMSU and AMSU-weighted MIPAS. As
 298 in Fig. 2, the MIPAS results are offset with respect to AMSU, with the magnitude of
 299 the offsets again all being less than 1 K. As seen with SSU, there is very good
 300 agreement between MIPAS and AMSU for the seasonal cycle, but with MIPAS
 301 exhibiting stronger cooling in the upper three channels (12-14). We will discuss this
 302 trend difference in Section 3.2 when we compare the trends to MLS.

303

304 **3.1.2 Algorithm for merging SSU and AMSU**

305 Since the SSU and AMSU weighting functions differ in shape and height of the maxi-
 306 ma, the two data sets must be combined by taking suitably weighted averages of the
 307 different channel temperatures. One way this might be done would be purely statis-
 308 tically, fitting the deseasonalized temperatures of instrument A to instrument B
 309 using multiple linear regression as follows

$$310 \quad \hat{T}_n^A(t) = \sum_{m=m_1}^{m_2} \alpha_m T_m^B(t) \quad (2)$$

311 where \hat{T}_n^A (with the hat) denotes the fitted deseasonalized temperature from
 312 channel n of instrument A, T_m^B denotes the actual deseasonalized temperature from
 313 channel m of instrument B, and the constants α_m are the coefficients determined
 314 using a least squares fit. However, this method, which we shall refer to as the
 315 temperature-fit method, is problematic because the time series used in computing
 316 the fit (T_m^B) are highly linearly dependent, as is shown in Fig. 4 in the case where
 317 B=AMSU. The top panel shows the deseasonalized temperature anomalies for the six
 318 channels superimposed. Adjacent or near-adjacent channels are highly correlated.
 319 Given the overlap in the AMSU weighting functions (W), some correlation is to be
 320 expected. For example, for the highest three channels the overlap between W_{13} and
 321 W_{14} is $\sim 61\%$, between W_{12} and W_{13} is $\sim 60\%$ and between W_{12} and W_{14} is $\sim 31\%$.

322 However, the fact that the correlations are actually close to unity for those pairs of
 323 channels, i.e., $r(13,14)\sim 0.96$, $r(12,13)\sim 0.96$ and $r(12,14)\sim 0.88$, suggests that they
 324 also reflect strong vertical relationships in the variability of global-mean
 325 temperature. A similarly high correlation of 0.91 is found between channels 9 and
 326 10, while channel 11 is highly correlated with both channel 10 ($r\sim 0.90$) and channel
 327 12 ($r\sim 0.87$). Thus, there appear to be only two degrees of freedom among the six
 328 channels, representing the upper stratosphere and the lower stratosphere. Similarly
 329 high correlations are found, albeit with more noise, in the CMAM30 data shown in
 330 the bottom panel of Fig. 4, which is plotted over the 1979 to 2011 period. The high
 331 correlations between the different channel temperatures means that the system of
 332 equations defined by Eq. (2) is highly underconstrained, and that there are no
 333 unique values of the coefficients α_m . This was verified in a calculation in which one
 334 of the α_m 's was specified and the remaining ones were computed, which yielded an
 335 almost identical temperature time series yet with very different coefficients. For this
 336 reason the temperature-fit method will not be used.

337 An alternative method, which is the method we have adopted, is to determine the fit
 338 coefficients from the weighting functions. Such a method has also been examined by
 339 the Remote Sensing Systems group, which has processed and combined the SSU
 340 data (C. Mears, personal communication, 2014). Using the weighting functions to
 341 generate the temperature fit coefficients makes physical sense since it is the chan-
 342 nels of instrument B that have weighting functions peaking closer to the peak of a
 343 given weighting function of instrument A that should be given the most weight in
 344 the fit. Another advantage of this method is that it does not require the two
 345 temperature data sets to overlap in time, as does the temperature-fit method.

346 The weighting function fit method proceeds as follows. We first express the channel-
 347 n weighting function of instrument A as a linear combination of the weighting
 348 functions of instrument B:

$$349 \quad \widehat{W}_n^A(z) = \sum_{m=m_1}^{m_2} \beta_m W_m^B(z) \quad (3)$$

350 where the hat denotes the fitted weighting function. The constants β_m are computed
 351 using least squares and are normalized so that $\sum_{m=m_1}^{m_2} \beta_m = 1$. The deseasonalized
 352 temperatures for channel n of instrument A are then constructed as follows

$$353 \quad \hat{T}_n^A(t) = c_n + \sum_{m=m_1}^{m_2} \beta_m T_m^B(t) \quad (4)$$

354 where the constants c_n represent an additive relative bias between the two
 355 measurements.

356 The dotted curves in the left panel of Fig. 1 are the fits to the three SSU weighting
 357 functions using the six AMSU weighting functions ($m_1=9$ and $m_2=14$), computed
 358 using Eq. (3), but before the β_m 's are normalized. The values of the unnormalized
 359 β_m 's are given in Table 2. The reason that they do not sum to unity is due to
 360 incomplete sampling of the target weighting function. As seen in Fig. 1 the fits to SSU
 361 channels 1 and 2 are excellent, with the only significant departures from the true
 362 weighting function occurring below ~ 10 km and above ~ 50 km where the SSU
 363 weighting functions do not have much strength anyways. Not surprisingly, the fit is
 364 poorest for the upper SSU channel 3 since there are no AMSU weighting functions
 365 that peak above it. The corresponding fits using the normalized β_m 's are given by the
 366 thin solid curves.

367 The reason for normalizing the β_m 's becomes apparent by considering the case of a
 368 constant temperature T_o profile with an assumption of no relative bias between
 369 instruments A and B, in which case it can be easily shown that

$$370 \quad c_n = T_o(1 - \sum_{m=m_1}^{m_2} \beta_m). \quad (5)$$

371 Since we have assumed no relative bias between the two instruments, c_n should
 372 vanish. This will only occur if $\sum_{m=m_1}^{m_2} \beta_m = 1$.

373 To compute c_n we use temperatures from a third instrument (C), which overlaps in
 374 time with instruments A and B and is of high enough vertical resolution that a
 375 sufficiently accurate representation of the temperatures obtained from the
 376 weighting functions of both instruments A and B can be computed. In this case,
 377 instrument C provides a transfer function between instruments B and A, whereby c_n
 378 can be expressed as the sum of three biases, namely,

379
$$c_n = E_{A-C} + E_{C-B} + E_W \quad (6)$$

380 where

381
$$E_{A-C} \equiv \langle T^A \rangle - \langle T^{AC} \rangle \quad (7)$$

382
$$E_{C-B} \equiv \sum_m \beta_m [\langle T_m^{BC} \rangle - \langle T_m^B \rangle] \quad (8)$$

383
$$E_W \equiv \langle T^{AC} \rangle - \sum_m \beta_m \langle T_m^{BC} \rangle \quad (9)$$

384 where the angled brackets denote a time average, and, as before, all temperatures
 385 are deseasonalized. For clarity, we have omitted the subscript n since it is common
 386 to all terms. The quantities T^{AC} and T^{BC} denote the temperatures of instrument C
 387 that have been averaged in the vertical using the weighting functions for instru-
 388 ments A and B, respectively. The first term (E_{A-C}) in Eq. (6) denotes the relative bias
 389 between the temperature of instrument A and the instrument A-weighted tempera-
 390 ture of instrument C. The second term (E_{C-B}) is the same but for instrument B (with a
 391 minus sign), where the summation over m is required since we are computing the
 392 temperature bias for channel n of instrument A. The third term (E_W) is the weighting
 393 function bias, which accounts for the error in the fits to the weighting functions; this
 394 term must be evaluated using the height-dependent temperatures from instrument
 395 C. If the period over which the time averages of the different terms in Eq. (6) are
 396 computed is the same, then

397
$$c_n = \langle T^A \rangle - \sum_{m=m_1}^{m_2} \beta_m \langle T_m^B \rangle \quad , \quad (10)$$

398 in which case instrument C is not needed. The advantage of Eq. (6) over Eq. (10),
 399 however, lies in the fact that instrument C enables us to separate the relative biases
 400 into different components. Moreover, if there is a gap in time between instruments
 401 A and B, but instrument C still overlaps with instruments A and B, then Eq. (10)
 402 could not be used.

403

404 **3.1.3 Merging SSU and AMSU using MIPAS**

405 Here we consider only the case where we extend SSU forward in time, which means
 406 that A=SSU and B=AMSU in Eq. (4). While it is certainly possible to extend AMSU
 407 backward (i.e., A=AMSU and B=SSU), we do not do so because the weighting func-

408 tion bias terms (E_W) are substantially larger when fitting the three broad SSU
409 weighting functions to the six narrower AMSU weighting functions.

410 Table 3 shows the different bias terms given in Eq. (6), which are used to compute c_n
411 in Eq. (4). The bottom row lists the sum of the three biases, which are the c_n 's. The
412 magnitudes of the individual bias terms are all less than 1.2 K, with some cancel-
413 lation between the different terms. The $E_{SSU-MIPAS}$ term is identical to the offsets
414 between SSU and SSU-weighted MIPAS shown in Fig. 2. The weighting function term
415 E_W is largest for channel 3 since the fit is the poorest (see Fig. 1). Figure 5 shows the
416 difference between the deseasonalized SSU temperatures and the fitted tempera-
417 tures computed using AMSU as a function of time, and indicates that the relative
418 biases (whose means are the c_n 's) are fairly stable in time. The standard deviations
419 of the differences, which provide a conservative measure of the uncertainty of the
420 fits, are 0.06, 0.09 and 0.09 K for channels 1, 2 and 3, respectively. These values are
421 clearly much smaller than the dynamic range seen in Fig. 6, which shows the SSU
422 data (black) and the corresponding extension derived from AMSU and MIPAS using
423 Eqs. (4) and (6) for the 1979-2012 time period. These fit uncertainties have been
424 propagated into our trend uncertainties; the effects are small although not entirely
425 negligible for the 1980-2012 period. The insets show blow-ups of the two time
426 series in the overlap period, along with the corresponding correlation coefficients r .
427 The agreement between the two time series is very good, with the highest cor-
428 relation occurring for the lowest channel. Even for channel 3, where the fit to the
429 weighting function is the poorest, the correlation coefficient is 0.895, which suggests
430 that the global-mean temperature variations in this region are vertically coherent.

431 The SSU and fitted SSU deseasonalized temperature time series can be combined
432 into a single time series, which we shall refer to as the “extended SSU” time series
433 \tilde{T}_n^{SSU} (denoted with a tilde), as follows

$$434 \quad \tilde{T}_n^{SSU} = \alpha(t)T_n^{SSU} + \beta(t)\hat{T}_n^{SSU} \quad (11)$$

435 where \hat{T}_n^{SSU} is the time series computed using Eqs. (4) and (6), and the time-depen-
436 dent coefficients α and β are given by

$$\begin{aligned}
437 \quad & \alpha(t) = 1 && \text{for } t \leq t_1 \\
438 \quad & \alpha(t) = 1 - \frac{(t-t_1)}{(t_2-t_1)} && \text{for } t_1 \leq t \leq t_2 \\
439 \quad & \alpha(t) = 0 && \text{for } t \geq t_2
\end{aligned}$$

440 and $\beta = 1 - \alpha$ where $t_1 = 2001.00$ and $t_2 = 2006.25$ are the start and end dates of the
441 overlap period between SSU and AMSU channel 14. The extended SSU temperatures,
442 expressed as anomalies with respect to the 1979-82 mean, are shown in Fig. 7 (red
443 curves). The other curves in this figure will be discussed in the next section.

444

445 **3.2 Stratospheric temperature trends**

446 In this section we take a closer look at the temperature trends in the first decade of
447 this century using not only the AMSU and MIPAS data, but also MLS. We then take a
448 step back and re-examine the long-term trends in the context of model simulations.

449 Figure 8 compares AMSU temperatures (black) to the AMSU-weighted results com-
450 puted from MIPAS (blue) and MLS (red), with the latter two being offset with
451 respect to AMSU for display purposes. The offsets are computed so that the time
452 means in the overlap period are identical to those of AMSU. As remarked earlier, the
453 AMSU-weighted MIPAS temperatures exhibit stronger cooling in the upper channels
454 than do AMSU. MIPAS is known to have a drift due to time-dependent detector-non-
455 linearity, which had not been considered for the calibration of radiance spectra used
456 here (e.g., Eckert et al., 2014). A latitude and altitude dependent drift of MIPAS tem-
457 peratures relative to MLS of the order of -1 K decade^{-1} has been identified for most
458 parts of the stratosphere (Eckert, 2012), which is in agreement with the trend dif-
459 ferences found here. A refined calibration, which takes the time-dependence of the
460 detector-nonlinearity into account, is currently under investigation. The MLS
461 results, however, do not show such an effect, and are in fact in better agreement
462 with AMSU on a year-to-year basis.

463 The temperature trends from MIPAS and MLS computed from 2004-12 are shown in
464 Fig. 9 as a function of height. Two types of uncertainties are shown. The first
465 assumes the data points are independent (thick error bars and dark shading); this is

466 appropriate when comparing trends between different data sets over the same time
467 period, where the differences will be mainly instrumental. The second takes into
468 account serial correlation using the lag-1 autocorrelation coefficient to estimate the
469 reduced number of degrees of freedom following Santer et al. (2000) (thin error
470 bars and light shading). Since serial correlation is a property of the atmosphere, not
471 of a particular instrument, the lag-1 autocorrelation coefficient computed from the
472 MLS data is used in calculating the reduced number of degrees of freedom for the
473 sparser MIPAS data. Although the time period is relatively short, global-mean
474 temperature exhibits limited internal variability (since it is under radiative control)
475 and so the uncertainties in the trends in the upper stratosphere are relatively low.
476 Superimposed on Fig. 9 are the AMSU trends (black circles) and the AMSU-weighted
477 MLS and MIPAS trends (black squares). The weighted trends are seen to lie along a
478 vertically smoothed version of the profile trends. As was seen in Fig. 8, the
479 agreement between MLS and AMSU is excellent (left panel), while MIPAS shows
480 substantially stronger cooling trends in the upper stratosphere (right panel). The
481 same conclusions can be inferred from the trends from extended SSU (red circles)
482 and SSU-weighted MLS and MIPAS (red squares), computed for the 2004-2012
483 period, which are also shown on Fig. 9.

484 Although MLS uses as its a priori an analysis that has assimilated AMSU radiances,
485 the impact of AMSU on the MLS temperatures is thought to be relatively small since
486 the MLS retrievals are more susceptible to vertical variations much shorter than the
487 widths of the AMSU weighting functions (M. Schwartz, personal communication,
488 2014). We therefore believe that the good agreement between MLS and AMSU is
489 real and therefore an independent validation of the MLS data, while the strong
490 cooling in the MIPAS data is attributed to its known drift. It is not clear whether the
491 zig-zag vertical structure seen in the MLS profile trends is real, and we note that the
492 model trends (cf. Fig 10) do not exhibit such a structure.

493 We now return to Fig. 7, which shows the extended SSU temperature anomalies
494 (with respect to 1979-82) plotted from 1979 to 2012, along with those from the

495 CMIP5 models. Near-global mean model temperatures are constructed from
496 monthly means and vertically averaged using the SSU weighting functions using Eq.
497 (1), with the limits of integrations being $z_b=0$ km and z_t = the height corresponding
498 to the top pressure level provided by each model data file, normalizing the
499 weighting functions to have a vertical integral of unity over the data height range. As
500 explained in Sect. 2.6 (see also Table 1), the CMIP5 models with poor vertical
501 resolution in the stratosphere are not projected onto all three SSU channels, which
502 explains why more gray curves are present in the bottom panel than in the top
503 panel. The agreement between the CMIP5 multi-model mean (black) and extended
504 SSU (red) is remarkably good. The good agreement from 1979 to 2006 has arisen, of
505 course, because we are using Version 2 of the NOAA SSU data. However, as noted
506 earlier Zou et al. (2014) did not compare SSU Version 2 to models; here we do. After
507 2006 (the end of the SSU data record) the extended SSU temperatures also compare
508 favourably with the CMIP5 models, with both exhibiting continued stratospheric
509 cooling followed by warming starting in about 2009. The cooling is due to a
510 combination of the effects of increasing CO₂ and the declining phase of the previous
511 solar cycle, while the warming is presumably due to the current solar cycle which
512 commenced in 2008. Note that the CMIP5 RCP simulations included a solar cycle by
513 repeating the last solar cycle (1996-2008) into the future.

514 Figure 10 compares the long-term temperature trends for extended SSU and the
515 CMIP5 models (1980-2012; left) and for extended SSU and the CCMVal2 models
516 (1980-2005; right). For 1980-2012 the trends for extended SSU are 0.63 ± 0.13 , -
517 0.71 ± 0.15 and -0.80 ± 0.17 K decade⁻¹ for channels 1, 2 and 3, respectively. The
518 95% uncertainties, which are computed the same way as in Fig. 9, take into account
519 serial correlation. The extended SSU cooling trends for 1980 to 2005 are ~ 9%
520 larger than those for 1980-2012 for channel 1 and ~ 15% larger for channels 2 and
521 3. This reflects the much weaker cooling rate over the second half compared with
522 the first half of the extended record. In all cases, the SSU-weighted model trends
523 (squares) agree with the observed trends within the uncertainties (error bars). The
524 cooling increases with increasing altitude for both the models and the observations.

525 Although the channel 3 extended SSU trend is considerably weaker than the
526 CCMVal2 trend profile at the altitudes where the weighting function peaks (~44
527 km), the channel 3 CCMVal2 trend is entirely consistent with the extended SSU
528 trend. This difference between the weighted and profile trend is due to the large
529 curvature in the profile trend. This illustrates why nadir measurements should
530 never be directly compared with profile measurements. For the CMIP5 models the
531 curvature of the profile trend is much weaker than for the CCMVal2 models, which
532 explains why the weighted and profile trends are in much closer agreement. The
533 lack of strong cooling above ~40 km in the CMIP5 models is presumably a result of
534 coarser stratospheric resolution and lower upper boundaries than the CCMVal2
535 models, which also have more comprehensive physical parameterizations for the
536 middle atmosphere.

537 Figure 11 shows near-global mean temperature differences for extended SSU and
538 the CCMVal2 multi-model means for the period of strong ozone depletion (1986-
539 1995; left) and the start of ozone recovery (1995-2004; right). (Note that for these
540 periods, the merging is irrelevant and the comparison is basically with the Version 2
541 NOAA SSU record itself.) We prefer differences to linear trends for this purpose
542 because of the highly nonlinear time evolution. To minimize the impact of solar
543 variability, which clearly has a large modulating effect on the long-term cooling (e.g.
544 Fig. 7), we compare the two recent decadal periods between solar minima. For
545 extended SSU, distinct cooling of about -0.7 K is seen at all levels over 1986-1995,
546 whereas negligible cooling is found over 1995-2004. This highlights the important
547 role of ozone depletion in the observed stratospheric cooling up to the mid-1990s. A
548 similar though somewhat less pronounced contrast between the two periods is seen
549 in the temperature differences from the models.

550 **4 Conclusions**

551 We present a physically based method for merging near-global mean brightness
552 temperatures from SSU and AMSU using measurements from a third instrument, in
553 this case MIPAS, which has high enough vertical resolution that it can sufficiently

554 accurately simulate the vertically weighted temperatures of both SSU and AMSU.
555 The SSU temperatures are expressed as a linear combination of AMSU temperatures,
556 with the coefficients determined by fitting the AMSU weighting functions to the SSU
557 weighting functions. The MIPAS data is used in matching the SSU temperatures and
558 the AMSU-simulated SSU temperatures.

559 Multiple linear regression does not work for merging the SSU and AMSU tem-
560 peratures because the AMSU channels are not sufficiently linearly independent (in a
561 statistical sense) and thus the determination of the regression coefficients is under-
562 constrained. Part of the correlation between the channels arises from the overlap of
563 the weighting functions, but part reflects strong vertical relationships in the
564 variability of global-mean temperature.

565 The relative bias between SSU and the AMSU-simulated SSU channels is expressed
566 as a sum of three relative biases: between SSU and MIPAS, between the SSU
567 channels and the AMSU-simulated SSU channels (both applied to MIPAS data), and
568 between MIPAS and AMSU. In this way, MIPAS is used as a transfer function
569 between SSU and AMSU.

570 In this particular case, SSU and AMSU overlap in time and so a transfer function is
571 not strictly required, but our method would be applicable in cases where the two
572 data sets to be merged did not overlap in time, so long as there was a higher
573 resolution data set that bridged between them. Also, this method allows for quanti-
574 fication of the error incurred by the approximation of the SSU weighting functions
575 by the AMSU weighting functions.

576 MIPAS was found to track the three SSU channels and the six AMSU channels very
577 well in time, especially in their seasonal cycle. This provides well-defined relative
578 biases between MIPAS and the two nadir instruments, allowing for the merging of
579 the two nadir records to be performed with confidence. In particular, the standard
580 deviation of the differences during the overlap period is less than 0.1 K for all three
581 SSU channels, which is much less than the dynamic range of the time series. Thus,

582 uncertainties in the merging make only a very small contribution to the
583 uncertainties in the long-term changes. The relative bias that results from imperfect
584 approximation of the SSU weighting functions by the AMSU weighting functions is a
585 significant contributor to the overall relative bias for SSU channels 1 and 2, and the
586 dominant contributor for channel 3. Although the relative bias for channel 3 seems
587 stable over the overlap period (e.g. the correlation coefficient between SSU channel
588 3 and the AMSU-simulated channel 3 is 0.895), it does introduce a potential
589 systematic uncertainty into the extension of SSU channel 3 into the future using
590 AMSU.

591 The coefficients β_m and relative biases c_n developed here can be used to
592 continuously extend the NOAA Version 2 SSU record forward in time using AMSU, as
593 the AMSU record lengthens.

594 The near-global mean linear temperature trends for the extended SSU data set for
595 1980-2012 are 0.63 ± 0.13 , -0.71 ± 0.15 and -0.80 ± 0.17 K decade⁻¹ for channels 1,
596 2 and 3, respectively. These trends are in agreement with those from CMIP5 model
597 simulations over this period.

598 Because global-mean temperature exhibits relatively little interannual variability,
599 compared to the temperature in particular latitude bands, trends can be determined
600 with confidence even over relatively short records. We analyze trends over the
601 period 2004-2012 when data from a second vertically resolved temperature data
602 set, Aura MLS, is available. While MLS temperature trends are essentially identical
603 to those of AMSU, the current version of MIPAS data shows a cooling trend relative
604 to AMSU, which is in agreement with preceding drift analyses (Eckert, 2012). This
605 does not compromise the use of MIPAS as a transfer function between SSU and
606 AMSU, because the relative biases are computed for a particular period, nor for the
607 use of MIPAS data to examine seasonal cycles and interannual variability. However,
608 this version of MIPAS temperature should not be used to determine long-term
609 trends. On the other hand, the high level of agreement between MLS and AMSU
610 provides confidence in both data sets for trend analysis. Over the 2004-2012 period

611 these data show a statistically significant cooling ranging from $\sim 0.6 \pm 0.3$ K dec⁻¹ for
612 channel 14 to $\sim 0.3 \pm 0.2$ K dec⁻¹ for channel 12, and no statistically significant
613 change for the three lowest channels 9, 10 and 11.

614 It is worth noting that even the narrower weighting functions that characterize the
615 AMSU channels, relative to the deeper weighting functions of the SSU channels,
616 strongly smooth the vertical structure seen in the MLS trends. Thus, nadir
617 measurements should never be compared with profile trends derived from higher
618 vertical resolution instruments or models; the latter must always be first filtered
619 through the weighting functions of the nadir measurements.

620 The long-term stratospheric near global-mean temperature record since 1979,
621 which is represented by the SSU channels, exhibits considerable temporal structure
622 associated with cooling from increasing CO₂ and from ODS-induced ozone depletion,
623 the effects of the solar cycle, and warming from volcanic eruptions. Version 2 of the
624 NOAA SSU record is found to be consistent with the behaviour seen in model simu-
625 lations. This is in contrast to the findings of Thompson et al. (2012), who examined
626 Version 1 of that data. In particular, the (extended) SSU record and the CCMVal2
627 models show the same contrast in cooling trends between the ozone depletion and
628 recovery periods, with weak cooling over 1995-2005 compared with the large
629 cooling seen in the period 1985-1995 of strong ozone depletion. The extended SSU
630 data show a continued cooling beyond the end of the SSU record, with a small
631 warming in the last few years (up to 2011) which is presumably associated with the
632 solar cycle. Both features are consistent with the high-top CMIP5 models. Thus, the
633 extended SSU global-mean temperature record constructed here, which covers
634 1979-2012, is consistent with physical expectations of the vertical structure and
635 temporal variations in the rates of stratospheric cooling over this period.

636 **Acknowledgements**

637 Funding for Charles McLandress and Andreas Jonsson was provided from the
638 European Space Agency. The authors thank Gloria Manney for providing the Aura

639 MLS data and also for helpful discussions. Charles McLandress thanks David
640 Plummer for providing some diagnostic code. The two reviewers are thanked for
641 their constructive comments.

642

643 **References**

- 644 Christy, J. R., Spencer, R. W., Norris, W. B., Braswell, W. D., and Parker, D. E.: Error
645 estimates of version 5.0 of MSU-AMSU bulk atmospheric temperatures. *J. Atmos.*
646 *Oceanic Technol.*, 20, 613–629, 2003.
- 647 Dee, D. P., Uppala, S. M., Simmons, A. J., Berrisford, P., Poli, P., Kobayashi, S., Andrae,
648 U., Balmaseda, M. A., Balsamo, G., Bauer, P., Bechtold, P., Beljaars, A. C. M., van de
649 Berg, L., Bidlot, J., Bormann, N., Delsol, C., Dragani, R., Fuentes, M., Geer, A. J.,
650 Haimberger, L., Healy, S. B., Hersbach, H., Hólm, E. V., Isaksen, L., Kållberg, P., Köhler,
651 M., Matricardi, M., McNally, A. P., Monge-Sanz, B. M., Morcrette, J.- J., Park, B.- K.,
652 Peubey, C., de Rosnay, P., Tavolato, C., Thépaut, J. N., and Vitart, F.: The ERA-Interim
653 reanalysis: configuration and performance of the data assimilation system, *Quart. J.*
654 *Roy. Meteor. Soc.*, 137, 553–597, doi:10.1002/qj.828, 2011.
- 655 Eckert, E., Drifts and Trends in MIPAS Temperature and Ozone Measurements,
656 *Diplomerbeit*, Karlsruhe Institute of Technology, 2012.
- 657 Eckert, E., von Clarmann, T., Kiefer, M., Stiller, G. P., Lossow, S., Glatthor, N.,
658 Degenstein, D. A., Froidevaux, L., Godin-Beekmann, S., Leblanc, T., McDermid, S.,
659 Pastel, M., Steinbrecht, W., Swart, D. P. J., Walker, K. A., and Bernath, P. F.: Drift-
660 corrected trends and periodic variations in MIPAS IMK/IAA ozone measurements,
661 *Atmos. Chem. Phys.*, 14, 2571–2589, 2014.
- 662 Fischer, H., Birk, M., Blom, C., Carli, B., Carlotti, M., von Clarmann, T., Delbouille, L.,
663 Dudhia, A., Ehhalt, D., Endemann, M., Flaud, J. M., Gessner, R., Kleinert, A., Koopmann,
664 R., Langen, J., López-Puertas, M., Mosner, P., Nett, H., Oelhaf, H., Perron, G.,
665 Remedios, J., Ridolfi, M., Stiller, G., and Zander, R.: MIPAS: an instrument for
666 atmospheric and climate research, *Atmos. Chem. Phys.*, 8, 2151–2188, 2008.
- 667 Fomichev, V. I: The radiative energy budget of the middle atmosphere and its para-
668 meterization in general circulation models, *J. Atmos. Sol.-Terr. Phys.*, 71, 1577–1585,
669 2009.

670 Hegglin, M. I., Tegtmeier, S., Anderson, J., Froidevaux, L., Fuller, R., Funke, B., Jones,
671 A., Lingenfelter, G., Lumpe, J., Pendlebury, D., Remsberg, E., Rozanov, A., Tooney, M.,
672 Urban, J., von Clarmann, T., Walker, K. A., Wang, R., and Weigel, K.: SPARC Data
673 Initiative: Comparison of water vapor climatologies from international satellite limb
674 sounders, *J. Geophys. Res.*, 118, 11,824–11,846, doi:10.1002/jgrd.50752, 2013.

675 Hegglin, M. I., Plummer, D. A., Shepherd, T. G., Scinocca, J. F., Anderson, J., Froidevaux,
676 L., Funke, B., Hurst, D., Rozanov, A., Urban, J., von Clarmann, T., Walker, K. A., Wang,
677 H. J., Tegtmeier, S., and Weigel, K.: Vertical structure of stratospheric water vapour
678 trends derived from merged satellite data, *Nature Geosci.*, 7, 768–776, 2014.

679 Intergovernmental Panel on Climate Change (IPCC): Climate Change 2013: The
680 Physical Scientific Basis, edited by Stocker, T. F., Qin, D., Plattner, G.- K., Tignor, M.,
681 Allen, S.K., Boschung, J., Nauels, A. , Xia, Y., Bex, V., and Midgley, P. M.,: Cambridge
682 University Press, New York, 1535 pp., 2013.

683 Livesey, N. J., Read, W. G., Froideveaux, L., Lambert, A., Manney, G. L., Pumphrey, H.
684 C., Santee, M. L., Schwartz, M. J., Wang, S., Cofield, R. E., Cuddy, D. T., Fuller, R. A.,
685 Jarnot, R. F., Jiang, J. H., Knosp, B. W., Stek, P. C., Wagner, P. A., and Wu, D. L.: Version
686 3.3 Level 2 data quality and description document. Tech. Rep. JPL D-33509, Jet
687 Propulsion Laboratory, <http://mls.jpl.nasa.gov>, 2011.

688 McLandress, C., Plummer, D. A., and Shepherd, T. G: Technical Note: A simple
689 procedure for removing temporal discontinuities in ERA-Interim upper
690 stratospheric temperatures for use in nudged chemistry-climate model simulations,
691 *Atmos. Chem. Phys.*, 14, 1547–1555, doi:10.5194/acp-14-1547-2014, 2014.

692 Mears, C. A., and Wentz, F. J.: Construction of the Remote Sensing Systems V3.2
693 atmospheric temperature records from the MSU and AMSU microwave sounders. *J.*
694 *Atmos. Oceanic Technol.*, 26, 1040–1056, 2009.

695 Nash, J. and Saunders, R., A review of Stratospheric Sounding Unit radiance
696 observations for climate trends and reanalyses. *Quart. J. Roy. Meteor. Soc.*,
697 DOI: 10.1002/qj.2505, 2015.

698 Randel, W. J., Shine, K. P., Austin, J., Barnett, J., Claud, C., Gillett, N. P., Keckhut, P.,
699 Langematz, U., Lin, R., Long, C., Mears, C., Miller, A., Nash, J., Seidel, D. J., Thompson,
700 D. W. J., Wu, F., and Yoden, S.: An update of observed stratospheric temperature
701 trends, *J. Geophys. Res.*, 114, doi:10.1029/2008JD010421, 2009.

702 Santer, B. D., Wigley, T. M. L., Boyle, J. S., Gaffen, J. S., Hnilo, J. J., Nychka, D., Parker, D.
703 E., and Taylor, K. E., Statistical significance of trends and trend differences in layer-
704 average atmospheric time series, *J. Geophys. Res.*, 105, 7337-7356, 2000.

705 Schwartz, M. J., Lambert, A., Manney, G. L., Read, W. G., Livesay, N. J., Froideveaux, L.,
706 Ao, C. O., Bernath, P. F., Boone, C. D., Cofield, R. E., Daffer, W. H., Drouin, B. J., Fetzer,
707 E. J., Fuller, R. A., Jarnot, R. F., Jiang, J. H., Jiang, Y. B., Knosp, B. W., Krüger, K., Li, J.-L.
708 F., Mlynchak, M. G., Pawson, S., Russell, J. M. III, Santee, M. L., Synder, W. V., Stek, P. C.,
709 Thurstans, R. P., Tompkins, A. M., Wagner, P. A., Walker, K. A., Waters, J. W., and Wu,
710 D. L.: Validation of the Aura Microwave Limb Sounder temperature and geopotential
711 height measurements, *J. Geophys. Res.*, 113, doi:10.1029/2007JD008783, 2008.

712 Shepherd, T. G., and Jonsson, A. I.: On the attribution of stratospheric ozone and
713 temperature changes to changes in ozone-depleting substances and well-mixed
714 greenhouse gases, *Atmos. Chem. Phys.*, 8, 1435–1444, 2008.

715 Shine, K. P., Bourqui, M. S., de Forster, P. M., Hare, S. H. E., Langematz, U., Braesicke,
716 P., Grewe, V., Ponater, M., Schnadt, C., Smith, C. A., Haigh, J. D., Austin, J., Butchart, N.,
717 Shindell, D. T., Randel, W. J., Nagashima, T., Portmann, R. W., Solomon, S., Seidel, D. J.,
718 Lanzante, J., Klein, S., Ramaswamy, V., and Schwartzkopf, M. D.: A comparison of
719 model-simulated trends in stratospheric temperatures, *Q. J. R. Meteorol. Soc.*, 129,
720 1565–1588, doi: 10.1256/qj.02.186, 2003.

721 Solomon, S., Rosenlof, K. H., Portmann, R. W., Daniel, J. S., Davis, S. M., Sanford, T. J.,
722 and Plattner, G.-K.: Contributions of stratospheric water vapor changes to decadal
723 variation in the rate of global warming, *Science*, 327, 1219–1222, 2010.

724 Stiller, G. P., Kiefer, M., Eckert, E., von Clarmann, T., Kellmann, S., García-Comas, M.,
725 Funke, B., Leblanc, T., Fetzer, E., Froideveaux, L., Gomez, M., Hall, E., Hurst, D., Jordan,
726 A., Kämpfer, N., Lambert, A., McDermid, I. S., McGee, T., Miloshevich, L., Nedoluha, G.,

727 Read, W., Schneider, M., Schwartz, M., Straub, C., Toon, G., Twigg, L. W., Walker, K.,
728 Whiteman, D. N., Validation of MIPAS IMK/IAA temperature, water vapor, and ozone
729 profiles with MOHAVE-2009 campaign measurements, *Atmos. Meas. Tech.*, 5, 289–
730 320, doi: 10.5194/amt-5-289-2012, 2012.

731 Thompson, D. W. J., Seidel, D. J., Randel, W. J., Zou, C.-Z., Butler, A. H., Mears, C., Osso,
732 A., Long, C., and Lin, R.: The mystery of recent stratospheric temperature trends,
733 *Nature*, 491, 692–697, doi:10.1038/nature11579, 2012.

734 von Clarmann, T., Glatthor, N., Grabowski, U., Höpfner, M., Kellmann, S., Kiefer, M.,
735 Linden, A., Mengistu Tsidu, G., Milz, M., Steck, T., Stiller, G. P., Wang, D. Y., Fischer, H.,
736 Funke, B., Gil-López, S., and López-Puertas, M.: Retrieval of temperature and tangent
737 altitude pointing from limb emission spectra recorded from space by the Michelson
738 Interferometer for Passive Atmospheric Sounding (MIPAS), *J. Geophys. Res.*, 108,
739 D23, doi: 10.1029/2003JD003602, 2003.

740 von Clarmann, T., Höpfner, M., Kellmann, S., Linden, A., Chauhan, S., Funke, B.,
741 Grabowski, U., Glatthor, N., Kiefer, M., Schieferdecker, T., Stiller, G. P., and Versick,
742 S.: Retrieval of temperature, H₂O, O₃, HNO₃, CH₄, N₂O, ClONO₂ and ClO from MIPAS
743 reduced resolution nominal mode limb emission measurements, *Atmos. Meas.*
744 *Techn.*, 2, 159–175, 2009.

745 Wang, D. Y., von Clarmann, T., Fischer, H., Funke, B., Gil-López, S., Glatthor, N.,
746 Grabowski, U., Höpfner, M., Kaufmann, M., Kellmann, S., Kiefer, M., Koukouli, M. E.,
747 Linden, A., López-Puertas, M., Mengistu Tsidu, G., Milz, M., Steck, T., Stiller, G. P.,
748 Simmons, A. J., Dethof, A., Swinbank, R., Marquardt, C., Jiang, J. H., Romans, L. J.,
749 Wickert, J., Schmidt, T., Russell III, J., and Remsberg, E.: Validation of stratospheric
750 temperatures measured by Michelson Interferometer for Passive Atmospheric
751 Sounding (MIPAS) on Envisat, *J. Geophys. Res.*, 110, D08301,
752 10.1029/2004JD005342, 2005.

753 Wang, L., and Zou, C.-Z.: AMSU-A-Only atmospheric temperature data records from
754 the lower troposphere to the top of the stratosphere, *J. Atmos. Ocean. Tech.*, 31,
755 808–825, doi:10.1175/JTECH-D-13-00134.1, 2014.

756 Wang, L., Zou, C.-Z., and Qian, H.: Construction of stratospheric temperature data
757 records from Stratospheric Sounding Units, *J. Clim.*, 25, 2931–2946,
758 doi:10.1175/JCLI-D-11-00350.1, 2012.

759 Wickert, J., Reigber, C., Beyerle, G., König, R., Marquardt, C., Schmidt, T., Grunwaldt,
760 L., Galas, R., Meehan, T. K., Melbourne, W. G., and Hocke, K.: Atmosphere sounding by
761 GPS radio occultation: First results from CHAMP, *Geophys. Res. Lett.*, 28, 3263–
762 3266, 2001.

763 World Meteorological Organization (WMO): Scientific Assessment of Ozone
764 Depletion: 2014, World Meteorological Organization, Global Ozone Research and
765 Monitoring Project – Report No. 55, 416 pp., Geneva, Switzerland, 2014.

766 Zou, C.- Z., Qian, H., Wang, W., Wang, L., and Long, C.: Recalibration and merging of
767 SSU observations for stratospheric temperature trend studies, *J. Geophys. Res.*, 119,
768 10.1002/2014JD021603, 2014.

769 Table 1: CMIP5 models used in this study. The number of ensemble members for the
 770 historical and RCP 4.5 experiments are listed in the second and third columns,
 771 respectively. The fourth column lists the SSU channels onto which the data are
 772 projected, which is determined by the height of the top data level: channel 1 (any
 773 model with data at 1 hPa), channels 1 and 2 (any model with data at pressure levels
 774 below 1 hPa), and channels 1-3 (any model with data at pressure levels below 0.1
 775 hPa).

776

Model	Historical	RCP 4.5	SSU channels
CanESM2	1	5	1
GFDL-CM3	5	1	1
HadGEM2-CC	3	1	1,2
MIROC4h	3	3	1
MIROC-ESM	3	3	1,2,3
MIROC-ESM-CHEM	1	9	1,2,3
MPI-ESM-LR	3	3	1,2,3
MPI-ESM-P	2	0	1,2,3
MRI-CGCM3	5	1	1,2,3

777

778

779

780 Table 2: Unnormalized coefficients β_m for AMSU channels $m=9-14$ of the fits to the three
 781 SSU weighting functions $n=1-3$ used in Eq. (3).

782

AMSU channel (m)	SSU (n=1)	SSU (n=2)	SSU (n=3)
14	0.018	0.313	0.786
13	0.114	0.300	-0.267
12	0.422	0.185	0.334
11	0.226	0.100	-0.117
10	0.146	0.048	0.098
9	0.053	0.021	-0.017

783

784

785

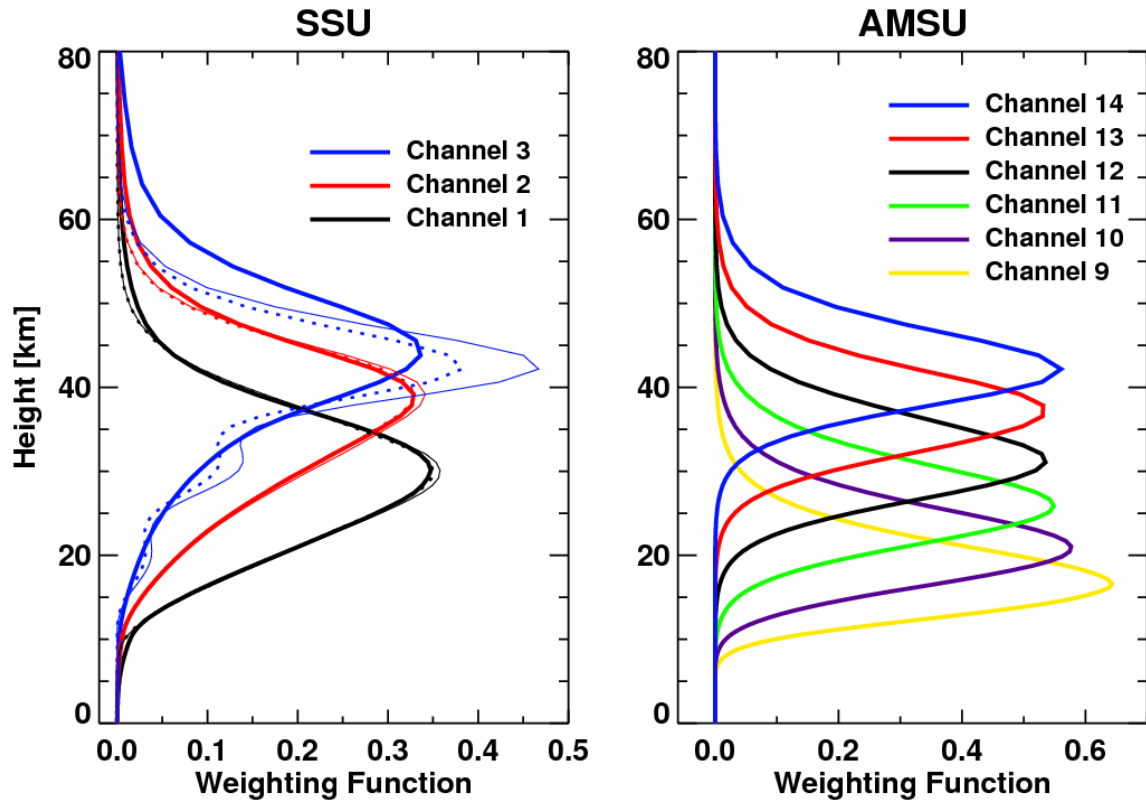
786

787 Table 3: The three bias terms in the expression for c_n in Eq. (6) for $n=1-3$ in the case
 788 where instrument A=SSU, B=AMSU and C=MIPAS. Units are K. The sum of the terms,
 789 which is listed in the bottom row, is the constant c_n used in Eq. (4). See text for
 790 details.

791

Bias	SSU (n=1)	SSU (n=2)	SSU (n=3)
$E_{SSU-MIPAS}$	-0.173	-0.744	-0.241
$E_{MIPAS-AMSU}$	0.087	0.007	-0.686
E_W	0.398	0.334	1.196
Sum (c_n)	0.312	-0.403	0.269

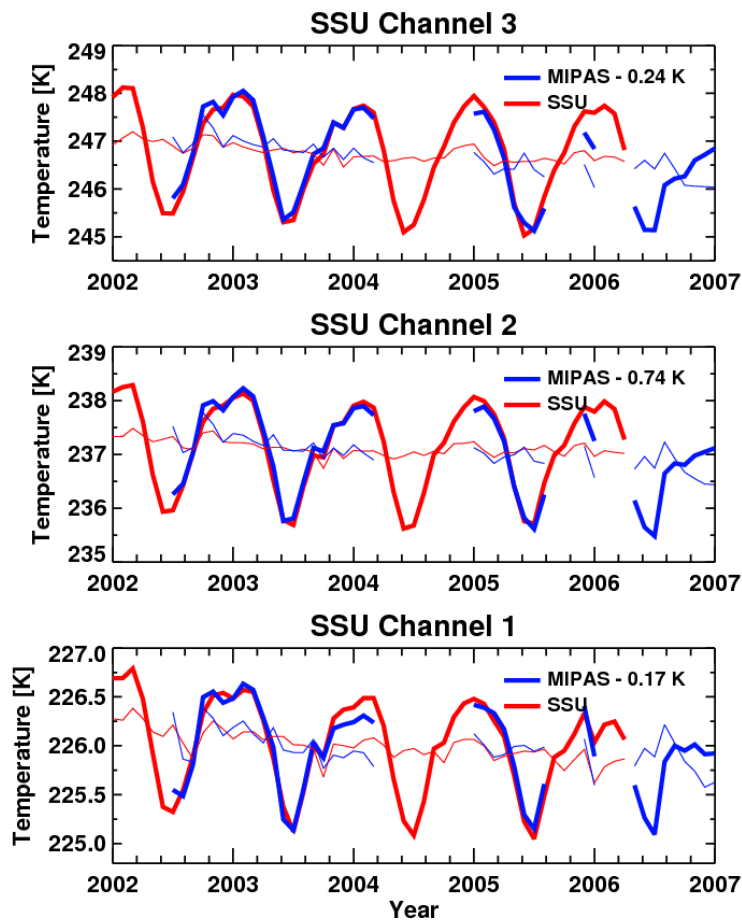
792



793
 794
 795
 796
 797
 798
 799

Figure 1: Vertical weighting functions (thick solid curves) for SSU (left) and AMSU (right). The thin solid and dotted curves in the left panel are, respectively, the normalized and unnormalized fits to the SSU weighting functions obtained using the AMSU weighting functions using Eq. (3); see text for details.

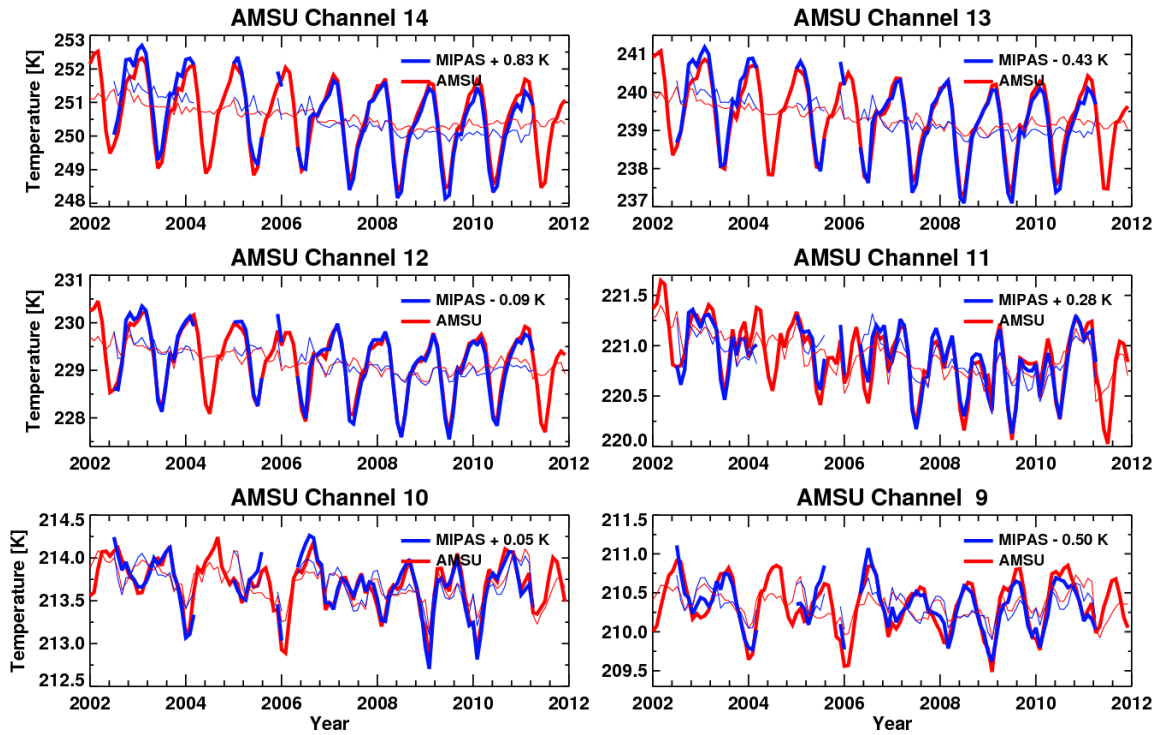
800
801
802
803
804
805
806
807



808
809
810
811
812
813
814
815
816
817

Figure 2: SSU (red) and SSU-weighted MIPAS (blue) temperatures for channels 1-3. The thin curves are the deseasonalized temperatures. The weighted MIPAS temperatures are offset by a constant amount so that the mean difference between the deseasonalized SSU and MIPAS time series is zero; the value of this offset is labeled in each panel. In this and all other figures, monthly and near-global (75°S-75°N) means are shown, and the tick marks directly above each year label on the horizontal axes are for January of that year.

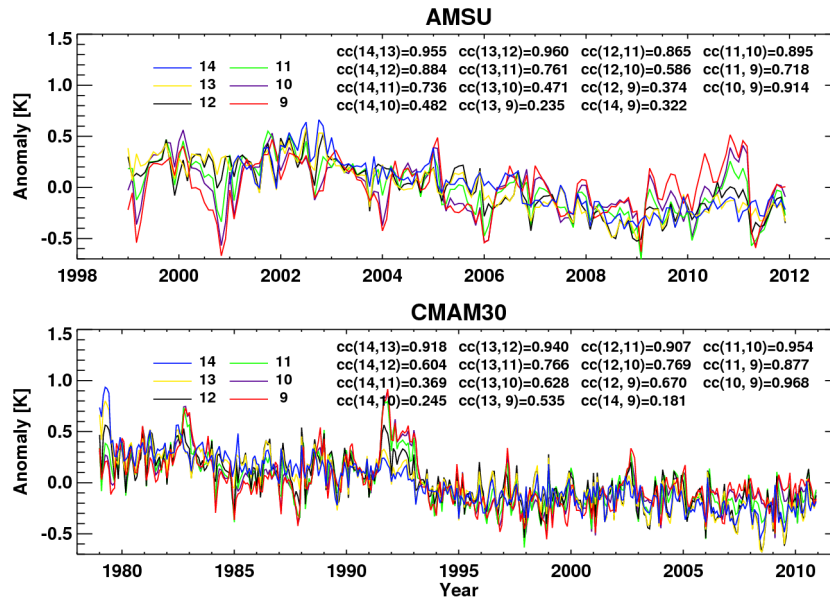
818
819
820
821
822
823
824
825
826



827
828
829
830
831
832

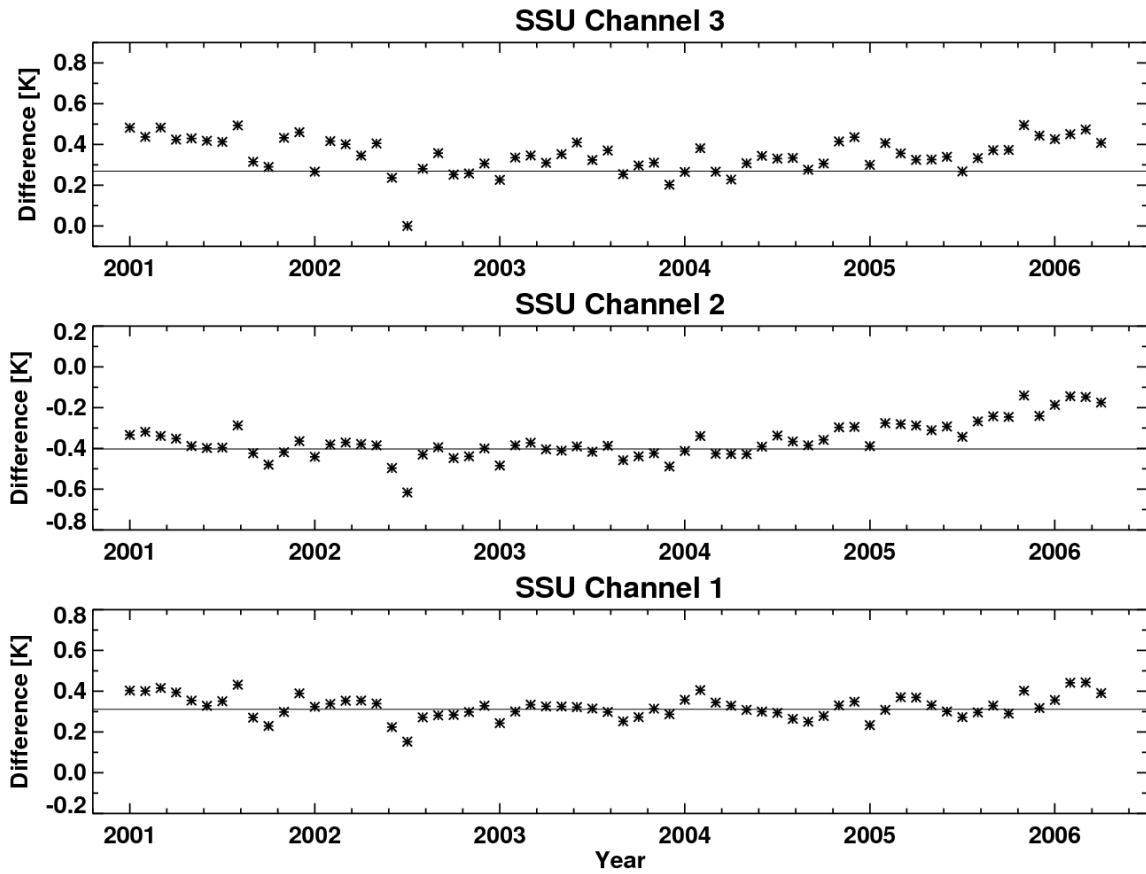
Figure 3: AMSU (red) and AMSU-weighted MIPAS (blue) temperatures for channels 9-14. The thin curves denote the deseasonalized temperatures. See the Fig. 2 caption for more details.

833
 834
 835
 836
 837
 838
 839



840
 841
 842
 843
 844
 845
 846
 847
 848
 849
 850
 851
 852
 853

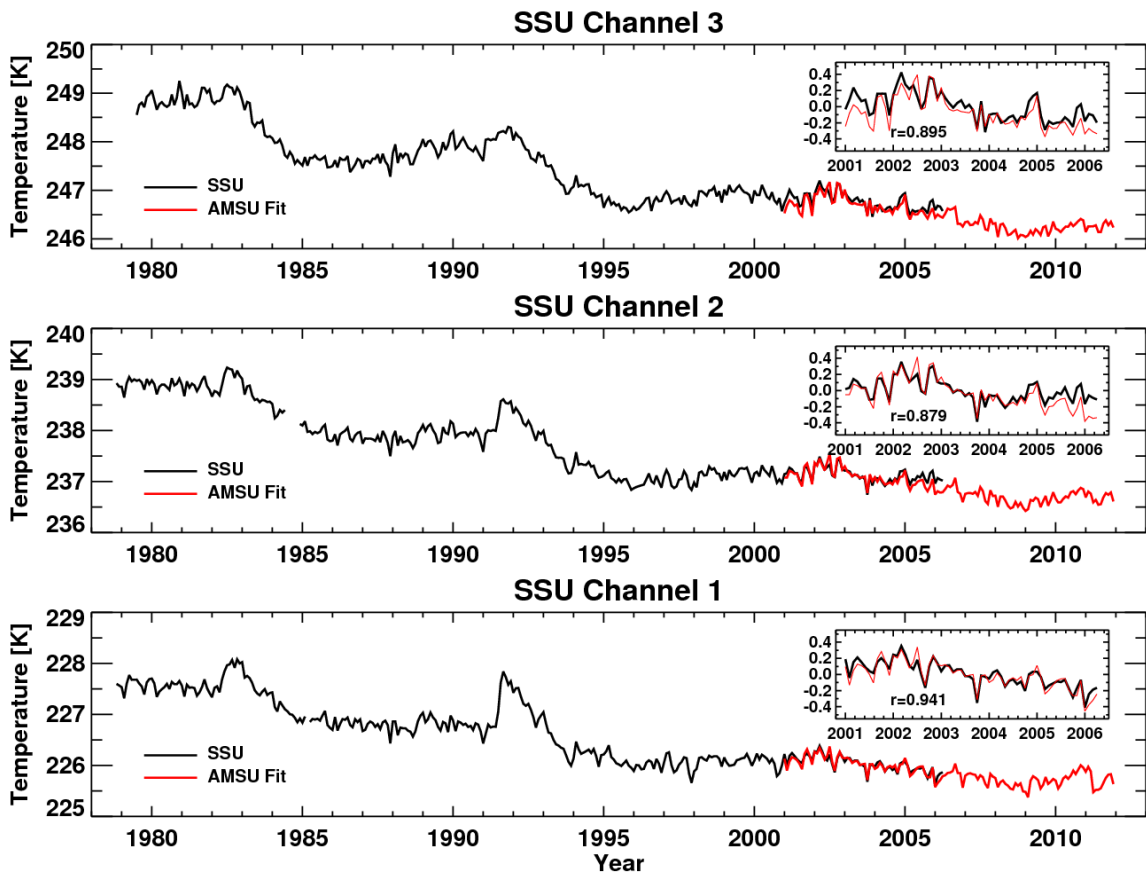
Figure 4: Top: Deseasonalized AMSU temperature anomalies with respect to the 1999-2011 mean for channels 9 to 13 and the 2001-2011 mean for channel 14, with the variance of each channel normalized to 0.25 K². Bottom: Same but for AMSU-weighted CMAM30 for the 1979 to 2011 time period. The correlation coefficient between the different channels is labeled in each panel.



854
 855
 856
 857
 858
 859

Figure 5: Difference between the deseasonalized SSU temperatures and the fitted temperatures computed using AMSU, i.e., $T_n^{SSU} - \sum_{m=m_1}^{m_2} \beta_m T_m^{AMSU}$. The horizontal lines are the constants c_n used in Eq. (4). See text for more details.

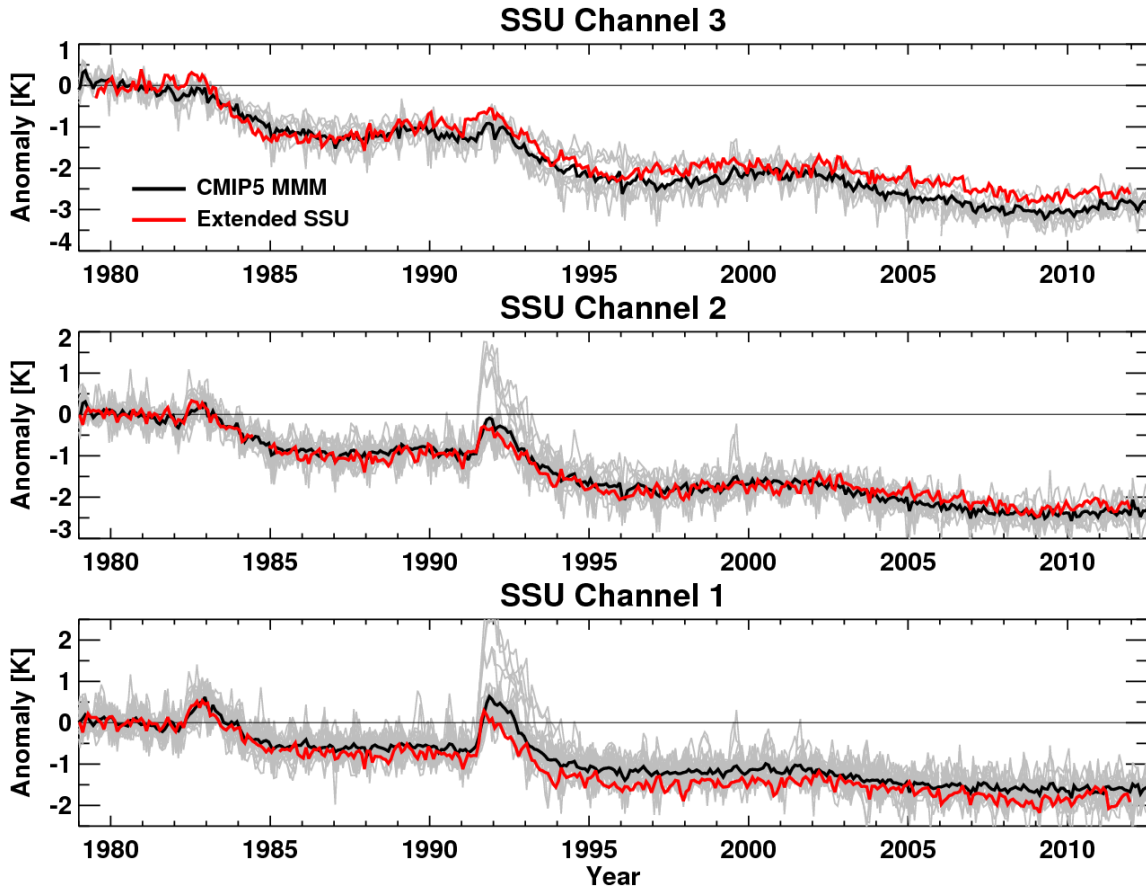
860
861
862
863
864
865
866
867
868



869
870
871
872
873
874
875

Figure 6: Deseasonalized temperatures for SSU channels 1-3 (black) and the fits computed from AMSU (red) using Eqs. (4) and (6). The insets show blow-ups of the time series in the overlap period (with the SSU time means subtracted off), along with the correlation coefficients (r) between each pair of curves.

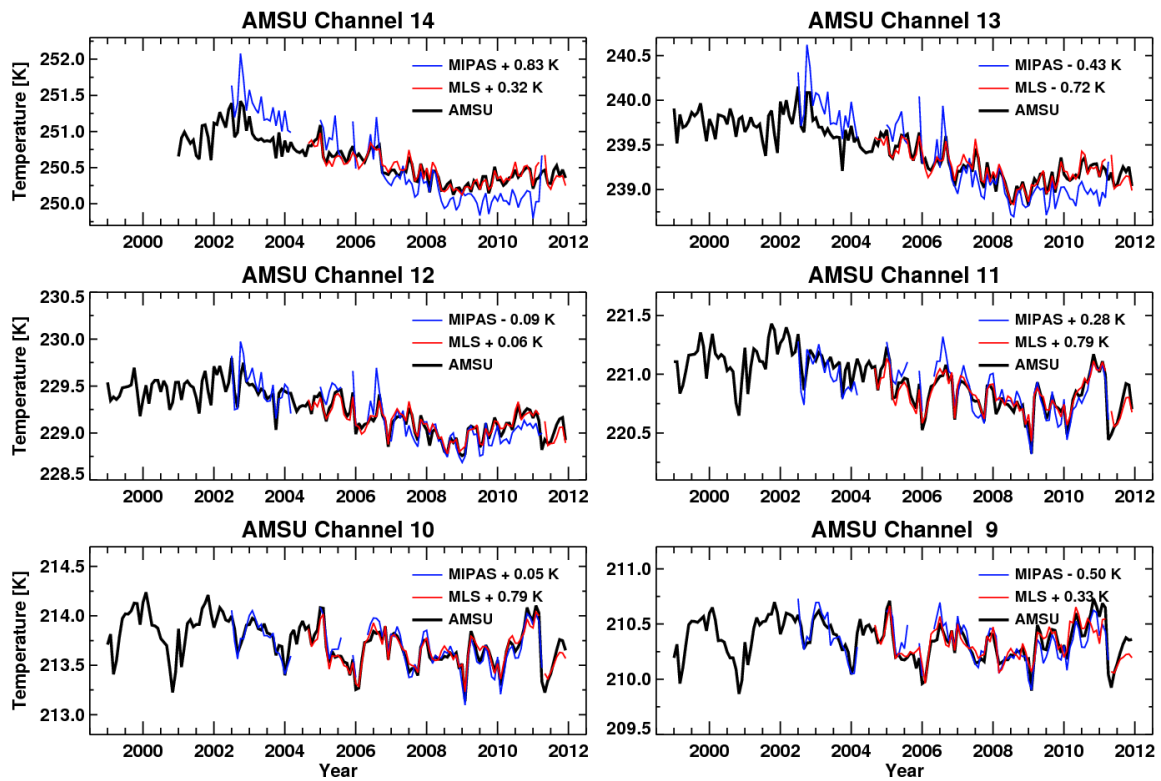
876
877
878



879
880
881
882
883
884
885
886

Figure 7: Deseasonalized temperature anomalies for extended SSU (red) and the CMIP5 multi-model mean (black). The light gray curves are the time series of the individual CMIP5 models used to compute the multi-model mean. Anomalies are computed with respect to 1979-82; thus the time mean anomaly over this period is zero.

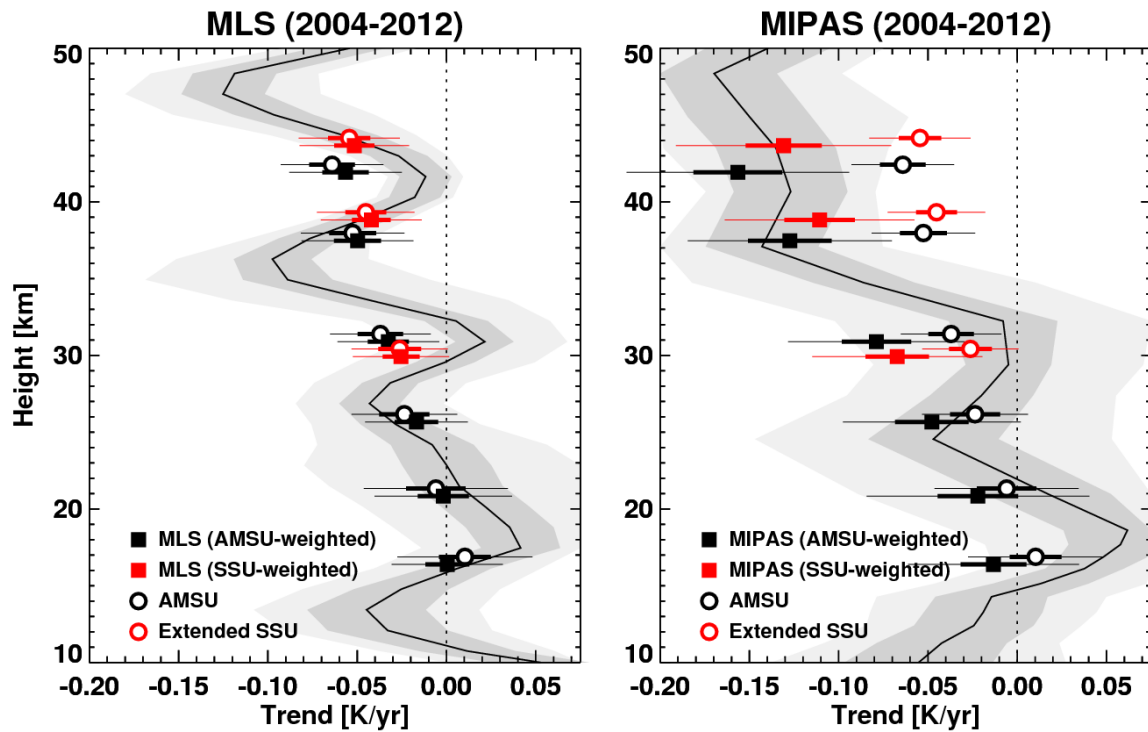
887
888
889
890
891
892
893
894



895
896
897
898
899
900
901

Figure 8: Deseseasonalized temperatures for AMSU channels 9-14 (black) and the corresponding AMSU-weighted temperatures computed from MIPAS (blue) and MLS (red). The constant offsets between MIPAS and AMSU and between MLS and AMSU are labeled in each panel.

902



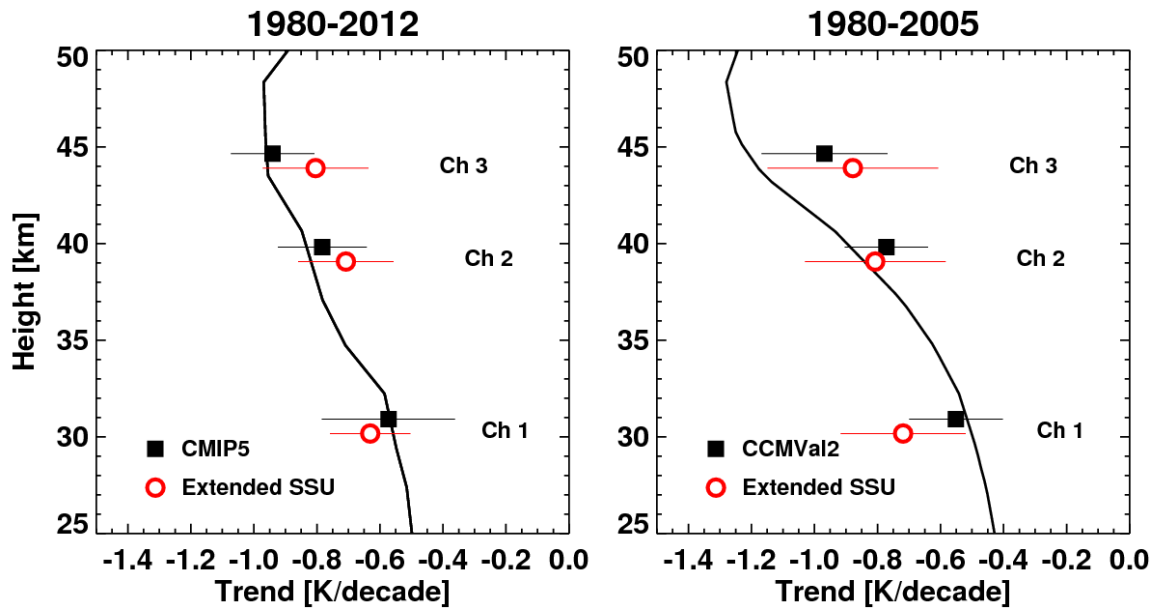
903

904

905 Figure 9: Linear temperature trends for MLS (left) and MIPAS (right) computed
906 from 2004-2012. The solid curves are computed from the height-dependent data;
907 the black and red squares are the corresponding AMSU-weighted and SSU-weighted
908 results plotted at the heights of the weighting function maxima shown in Fig. 1 and
909 offset slightly in the vertical for clarity. The black and red circles are the
910 corresponding trends from AMSU and extended SSU. The channel numbers range
911 from 14 (3) at the top to 9 (1) at the bottom for AMSU (SSU). The dark and light grey
912 shading, as well as the thick and thin error bars, denote the 95% confidence levels
913 computed assuming, respectively, independent and serially correlated data; see text
914 for details.

915

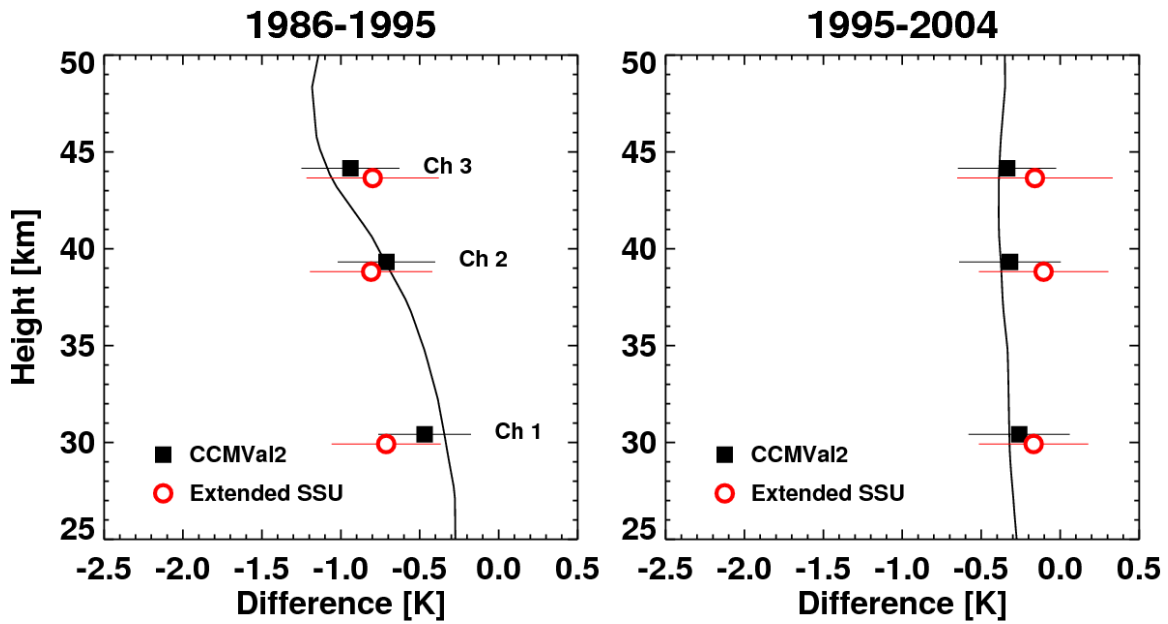
916



917
918

919 Figure 10: Temperature trends for extended SSU and the CMIP5 multi-model mean
920 for 1980-2012 (left) and extended SSU and the CCMVal2 multi-model mean for
921 1980-2005 (right). The trend profiles and weighted trends for the models are given
922 by the lines and squares. The latter are plotted at the heights of the maxima of the
923 three SSU weighting functions; for clarity the symbols for the models are offset
924 slightly with respect to extended SSU. The error bars denote the 95% confidence
925 levels.

926



927

928

929 Figure 11: Temperature differences for extended SSU and the CCMVal2 multi-model
 930 mean for 1986-1995 (left) and 1995-2004 (right). The CCMVal2 temperature
 931 difference profiles are given by the black curves, the SSU-weighted CCMVal2
 932 differences by the black squares and the extended SSU differences by the open
 933 circles. The latter two are plotted at the heights of the maxima of the three SSU
 934 weighting functions, ranging from channel 3 at the top to channel 1 at the bottom;
 935 the symbols are offset slightly in the vertical for clarity. The error bars denote the
 936 95% confidence levels. The differences are computed from data that have been
 937 averaged over two years spanning each of the two end points.